Theor Chem Acc (2011) 129:453–466
DOI 10.1007/s00214-010-0880-x

REGULAR ARTICLE

Calculation of molecular *g*-tensors using the zeroth-order regular approximation and density functional theory: expectation value versus linear response approaches

Jochen Autschbach · Benjamin Pritchard

Received: 28 October 2010 / Accepted: 17 December 2010 / Published online: 23 January 2011

Abstract Density functional theory (DFT) calculations of molecular *g*-tensors were implemented as a second derivative property within the two-component relativistic zeroth-order regular approximation (ZORA). *g*-tensors were computed for systems ranging from light atomic radicals to molecules with heavy *d* and *f* block elements. For comparison, computations were also performed with a ZORA first-order derivative approach and with a second derivative method based on the Pauli Hamiltonian. In each set of computations, Slater-type basis sets have been used. The new ZORA implementation allows for non-hybrid and hybrid DFT calculations. A comparison of the PBE non-hybrid and the PBE0 hybrid functional yielded mixed results for our test set. For the lanthanide complex $[Ce(DPA)_3]^{3-}$ (DPA = pyridine-2,6-dicarboxylate), calculations of the *g*-tensor were used to estimate paramagnetic NMR pseudocontact shifts for protons and carbon atoms in the ligands. The results are in reasonable agreement with experimental data.

Keywords Electron paramagnetic resonance · Density functional theory · Relativistic effects · Paramagnetic NMR

1 Introduction

The deviation of electronic *g*-values associated with the effective spin of a molecule from the free-electron *g*-factor of 2.0023 may be considered a purely relativistic effect [1] in the following sense: For such deviations to occur, there has to be spin-orbit (SO) coupling present. A coupling between spin and orbital angular momenta of electrons arises in relativistic theories of the electron. The electron *g*-tensor, or the *g*-shift tensor Δg which quantifies the deviation from the isotropic free electron case, is an important quantity in electron paramagnetic resonance (EPR) spectroscopy. EPR is one of the most versatile spectroscopic methods used to characterize radicals and transition metal ions with unpaired electrons [2–4]. The *g*-tensor has also been linked to a subset of the paramagnetic effects in the NMR of open shell molecules [5–8]. The word *g*-'tensor' is somewhat misleading due to the properties of *g* under coordinate transformations [3, 9, 10]. Nonetheless, we use the phrase '*g*-tensor' here because it is commonly used, with the understanding that it is gg^T, not *g* itself, that transforms as a rank 2 tensor.

There are different ways of calculating *g* and Δg. On the one hand, as was already pointed out by Abragam and Bleaney [3], a proper tensor related to the Zeeman interaction of the effective spin with an external magnetic field arises from considering the square of the spin Hamiltonian. This approach may be used to define *g*-tensor components as expectation values of the Zeeman Hamiltonian, without the need to solve response equations as long as SO coupling is variationally included in the calculation [9, 10]. Since expectation values of molecular properties other than the energy may be defined as first-order energy derivatives [11], in the context of this work we refer to this approach as the 'first order' or the 'expectation value' route to calculating the *g*-tensor. In the absence of SO coupling, i.e. in nonrelativistic theory, the *g*-tensor can be calculated from double perturbation theory [11] as a second-order energy derivative. One of the perturbations is the external

Dedicated to Professor Pekka Pyykkö on the occasion of his 70th birthday and published as part of the Pyykkö Festschrift Issue.

J. Autschbach (✉) · B. Pritchard
Department of Chemistry, State University of New York at Buffalo, Buffalo, NY 14260-3000, USA
e-mail: jochena@buffalo.edu

magnetic field. The other perturbation is the electron spin-orbit coupling, with the derivative formally being taken with respect to components of the effective spin vector occurring in the eigenvalues of the EPR spin Hamiltonian. In the context of this work, we refer to this approach as the 'second-order' or 'linear response' approach to calculating the *g*-tensor.

Different implementations based on nonrelativistic electronic structures that were reported up to 2001 have been discussed in Ref. [12]. Theoretical work directed at computing *g*-tensors based on ab-initio methods (Hartree-Fock, multi-configuration SCF, configuration interaction methods) or semiempirical wavefunctions has been reported, e.g., in Refs. [9, 13–18]. For further discussion of these approaches, we refer to the literature cited in Refs. [11, 12, 19]. For additional information and further references to pioneering work in this field as well as recent work, the reader is referred to the excellent overview articles by Patchkovskii and Schreckenbach [20], Neese [21], and Kaupp and Köhler [6]. For a discussion of various relativistic approaches, see also Ref. [22].

Instead of using a nonrelativistic computation as the starting point for a linear response calculation of the *g*-tensor, one may also employ a scalar relativistic (one-component) framework. For instance, Schreckenbach and Ziegler (SZ) [23] have adopted the Pauli operator in variational scalar relativistic DFT computations as a starting point for linear response *g*-tensor calculations. An application to d^1 transition metal complexes of the type MEX_4^{n-}, with M = V, Cr, Mo, W, Tc, and Re, E = O, N, and X = F, Cl, and Br was reported by Patchkovskii and Ziegler [24]. The computations have met with mixed success. Agreement between the computations and experiment was reasonable for the 3d and 4d metals, but the $\Delta g_{\|}$ component of the tensor was systematically overestimated for the 5d metals. Deficiencies have been attributed in to the tendency of commonly used non-hybrid functionals leading to overestimate the covalent character of the metal ligand bonds [24, 25]. Hybrid density functionals appear to perform somewhat better in comparison [12, 26]. More recently, Hrobárik et al. [27] have compared one- and two-component approaches and determined that, depending on the system, higher-order spin-orbit effects as well as choice of exchange-correlation function may significantly impact the accuracy of calculated *g*-tensors.

In relativistic DFT, a first-order (expectation value) route for variational calculations of the *g*-tensor has been implemented by van Lenthe, Wormer, and van der Avoird (LWA) [28] and successfully been applied to a large number of heavy atomic radicals [29]. The zeroth-order regular approximation (ZORA) two-component relativistic Hamiltonian has been used to treat scalar and SO relativistic effects. Malkin et al. [30] reported an implementation based on the Douglas–Kroll–Hess Hamiltonian where a particular focus has been on defining spin polarization in the two-component framework properly. Four-component methods have also been reported, for instance in Refs. [31, 32]. For a discussion of alternative ways to compute *g*-tensors in a relativistic wavefunction theory framework, and applications to molecules containing metal atoms as heavy as uranium or neptunium, see Refs. [33, 34].

This work is concerned with a direct comparison of the first-order and the second-order approach based on the same ZORA Hamiltonian and the same Slater-type orbital (STO) basis sets, within a relativistic density functional theory (DFT) framework. The *g*-tensor is more of a 'global' molecular property than shielding tensors or hyperfine tensors, and the desirable long-range behavior of STO basis functions should be advantageous for the computations. For systems with heavy elements, the first-order approach that includes SO coupling variationally, may be the more appealing one. Both the SZ second-order approach and the first-order approach of LWA have been implemented in the Amsterdam Density Functional (ADF) [35] package and therefore allow, in principle, for a direct comparison of first-order and the second-order methods for calculating *g*-tensors using the same Slater-type orbital (STO) basis sets, the same definitions of functionals, and the same numerical integration and other technical parameters. However, due to the variational instability of the Pauli operator, the relativistic linear response approach by SZ—which relies on the use of frozen core basis sets that are inflexible in the core region—is now deprecated. A direct comparison of the SZ method with all-electron ZORA calculations based on the LWA implementation for heavy element systems is therefore not possible. Other works have employed a combination of scalar relativistic DKH and Breit–Pauli SO Hamiltonians, along with Gaussian-type basis sets [27]. For this work, we have carried out a new implementation of the second-order approach for calculating *g*-tensors within the ZORA DFT framework. The implementation is part of the ADF package and allows a direct comparison with the results of the LWA approach using STO basis sets designed for ZORA computations. Details are provided in Sect. 2. For a test set of light and heavy atom radicals, it is shown here that in many cases both methods yield quite comparable results even for system with very heavy atoms (Sect. 4), although a breakdown of the second-order approach can be noted for linear molecules, in particular systems with heavy atoms such as HgF and HgH. Because one of the perturbations is an external magnetic field, care needs to be taken that the results, necessarily calculated with an incomplete basis set, are not origin dependent. The adoption of a gauge-including atomic orbital

(GIAO) basis set [36, 37] ensures origin independence of the g-tensors in the finite STO basis set calculations.

A second aim of this work is a comparison of non-hybrid with hybrid DFT in ZORA linear response calculations of g-tensors employing STO basis sets. Both the LWA and the SZ implementations have so far been restricted to non-hybrid functionals which, as pointed out above, can sometimes be a source of error in g-tensor calculations. The new second-order ZORA code takes advantage of some recent developments for ZORA-based calculations of NMR shielding tensors [38] and allows for computations with non-hybrid as well as with hybrid functionals. As an application of the new implementation, a third goal of this work is to evaluate the applicability of ZORA combined with DFT to computations of parameters relevant to the NMR of paramagnetic molecules. To this end, pseudocontact chemical shifts in the nine-coordinate Ce(III) complex $[Ce(DPA)_3]^{3-}$ (DPA = pyridine-2,6-dicarboxylate) are estimated with the help of computed g-tensor and chemical shift data.

Following this Introduction, the theoretical details of the ZORA linear response g-tensor calculations are provided in Sect. 2 along with some details about the implementation such as the numerical integration of the relevant perturbation operator matrix elements. Computational details are provided in Sect. 3. Calculated g-tensors for a number of light and heavy atomic systems are reported and discussed in Sect. 4. Paramagnetic NMR pseudocontact shifts for $[Ce(DPA)_3]^{3-}$ are also discussed in this section as an application of relativistic g-tensor calculations related to the NMR of open shell systems. This work concludes with a brief outlook in Sect. 5.

2 Theoretical background

2.1 Linear response g-tensors

One can define the components of the electronic g-tensor via a second derivative of the molecular energy, as done by Schreckenbach and Ziegler (SZ), Ref. [23]:

$$g_{uv} = \frac{1}{\beta_e}\frac{\partial^2 E}{\partial B_u \partial S_v} \tag{1}$$

Here, B_u is the component of an external magnetic field, and S_v is a component of the effective spin vector of the molecule. The Bohr magneton $\beta_e = e\hbar/(2m_e)$ enters the expression based on usual conventions for the EPR spin Hamiltonian [2]. In Dirac's theory of the electron, the free electron g_e is exactly 2. The difference between the Dirac value and the correct value of 2.0023 is due to QED corrections which we neglect here. Based on the Dirac value of g_e, in atomic units $g_e\beta_e = 1$. Since in the following we use atomic units and the Dirac equation, transformed to two components and approximated by ZORA, there is no electron g-factor present in the operators, but it is implicit in an 'overall factor' of $1 = g_e\beta_e$ atomic units which we may introduce back in the equations after the derivations are finished. The calculations determine the g-shifts Δg directly in which case it is not necessary to specify any particular value for g_e in the calculations. The free electron value can simply be added after the computation of Δg is complete.

Assuming either (1) a complete basis set or (2) a basis set that does not depend on the derivative parameters (which is not the case when a GIAO basis is used), the g-tensor components are in Kohn–Sham DFT double perturbation theory given *formally* (see Sect. 2.2) as

$$g_{uv} = \beta_e^{-1}\left\{\sum_i^{\text{occ}}\left\langle \varphi_i^{(0)}\middle|\hat{h}^{(u,v)}\middle|\varphi_i^{(0)}\right\rangle + 2\ \text{Re}\sum_i^{\text{occ}}\left\langle \varphi_i^{(u)}\middle|\hat{h}^{(v)}\middle|\varphi_i^{(0)}\right\rangle\right\} \tag{2}$$

where the perturbation operators are *formally* given by

$$\hat{h}^{(u)} = \frac{\partial \hat{h}(\boldsymbol{B},\boldsymbol{S})}{\partial \boldsymbol{B}_u} \tag{3a}$$

$$\hat{h}^{(v)} = \frac{\partial \hat{h}(\boldsymbol{B},\boldsymbol{S})}{\partial \boldsymbol{S}_v} \tag{3b}$$

$$\hat{h}^{(u,v)} = \frac{\partial^2 \hat{h}(\boldsymbol{B},\boldsymbol{S})}{\partial \boldsymbol{B}_u \partial \boldsymbol{S}_v} \tag{3c}$$

at zero field. The first operator does not occur explicitly in Eq. 2, but it is needed to calculate the perturbed orbitals $\varphi_i^{(u)}$ from the coupled-perturbed Kohn–Sham (CPKS) equations.

2.2 Taking the 'spin derivatives'

The spin component S_v in Eq. 1 is that of the effective spin assigned to the system in order to match the multiplicity of the resonances in the EPR experiment. In the absence of spin-orbit coupling, that is if the calculation is based on a nonrelativistic or scalar relativistic reference electronic structure, S_v is the maximum projection of the spin vector on a quantization axis in v direction. One may then choose the z direction arbitrarily and consider rotations of the coordinate system afterward, which yields the same maximum projection in the other directions, so it is sufficient to know S_z [23]. In a scalar relativistic spin-unrestricted Kohn–Sham DFT approach with singly occupied pure α and β spin orbitals,

$$S_z = \frac{n_\alpha - n_\beta}{2} \tag{4}$$

where n_α and n_β is the number of occupied orbitals of α and β spin, respectively.

The 'operator derivatives' in Eq. 2 with respect to spin-differentiation, and the resulting matrix elements, are not to be taken literally as written (unlike those for spin-free perturbation operators such as $\hat{h}^{(u)}$ that are commonly used to calculate molecular properties). Instead, Eq. 2 is a shorthand notation for the following: Consider a spin-dependent perturbation operator of the form

$$\hat{X}_z(\boldsymbol{r})\sigma_z$$

In a basis of nonrelativistic or spin-free scalar relativistic spin-orbitals, one has for an expectation value of the operator

$$\frac{\partial}{\partial S_z}\sum_i^{\text{all}}\left\langle \varphi_i^{(0)}\middle|\hat{X}_z\sigma_z\middle|\varphi_i^{(0)}\right\rangle = S_z^{-1}\left\{\sum_i^{\alpha\,\text{spin}}\left\langle \varphi_i^{(0)}\middle|\hat{X}_z\middle|\varphi_i^{(0)}\right\rangle - \sum_i^{\beta\,\text{spin}}\langle \varphi_i^{(0)}\middle|\hat{X}_z\middle|\varphi_i^{(0)}\rangle\right\} \tag{5}$$

As was pointed out above, the maximum spin projection is the same if another axis is chosen for the spin quantization axis. Therefore, when spin derivatives are calculated as above the spin-dependent part is the same, and one arrives at

$$\frac{\partial}{\partial S_v}\sum_i^{\text{all}}\left\langle \varphi_i^{(0)}\middle|\hat{X}_v\sigma_v\middle|\varphi_i^{(0)}\right\rangle = S_z^{-1}\left\{\sum_i^{\alpha\,\text{spin}}\left\langle \varphi_i^{(0)}\middle|\hat{X}_v\middle|\varphi_i^{(0)}\right\rangle - \sum_i^{\beta\,\text{spin}}\langle \varphi_i^{(0)}\middle|\hat{X}_v\middle|\varphi_i^{(0)}\rangle\right\} \tag{6}$$

along with an equivalent expression involving $\varphi_i^{(u)}$ for the 'paramagnetic' term of Eq. 2. The matrix elements of the derivative operators in Eq. 2 are taken in the sense of Eq. 6.

2.3 Perturbation operators in the ZORA formalism, nonrelativistic limits, and the Pauli approximation

We adopt a two-component relativistic theory in form of the zeroth-order regular approximation (ZORA) [39]. The ZORA one-electron Fock operator used in DFT with a local effective potential V reads in atomic units

$$\hat{h} = V + \frac{1}{2}(\vec{\sigma}\cdot\hat{\boldsymbol{p}})\mathcal{K}(\vec{\sigma}\cdot\hat{\boldsymbol{p}}) = V + \frac{1}{2}\hat{\boldsymbol{p}}\mathcal{K}\hat{\boldsymbol{p}} + \frac{1}{2}\imath\vec{\sigma}\cdot(\hat{\boldsymbol{p}}\mathcal{K}\times\hat{\boldsymbol{p}}) \tag{7}$$

where

$$\mathcal{K} = \frac{2c^2}{2c^2 - V} \tag{8}$$

is the function that regularizes the Hamiltonian around the nuclei and leads to the variational stability of the operator compared to, say, the Pauli Hamiltonian. In Eq. 7, $\vec{\sigma}$ is the 3-vector of 2×2 Pauli spin matrices, with components $\vec{\sigma} = (\sigma_x, \sigma_y, \sigma_z)$, and $\hat{\boldsymbol{p}} = -i\boldsymbol{\nabla}$ is the momentum vector operator.

The g-tensor is calculated based on orbitals obtained from a scalar ZORA variational calculation with the first two terms from the right-hand side of Eq. 7,

$$\hat{h}^{(0)} = V + \frac{1}{2}\hat{\boldsymbol{p}}\mathcal{K}\hat{\boldsymbol{p}} \tag{9}$$

That is, scalar (spin-free) relativistic effects are already contained in the unperturbed orbitals. For light atomic systems, these effects are small and scalar ZORA is essentially equivalent to a nonrelativistic calculation. The potential V in Eqs. 7 and 9 is obviously determined self-consistently for systems with more than one (spin) orbital and may be adapted for hybrid functionals to include exact exchange contributions. In order to simplify the calculations, and to avoid certain conceptual problems with ZORA, the potential V used to construct $\mathcal{K}$ in Eq. 8 is approximated as a sum of (local) atomic potentials V_A (SAPA), i.e. $V \approx \sum_A V_A$. This is an efficient and accurate approximation of ZORA and has been implemented in the ADF [40] and NWChem [41, 42] packages. A related approach was taken by van Wüllen for a ZORA implementation in the Turbomole code [43].

The operators that are dependent on magnetic fields are obtained from the minimal substitution

$$\hat{\boldsymbol{p}} \to \hat{\boldsymbol{p}} + \boldsymbol{A} \tag{10}$$

in the ZORA operator, Eq. 7. For a static external magnetic field, the vector potential $\boldsymbol{A}$ is

$$\boldsymbol{A} = \boldsymbol{B}\times\boldsymbol{U} \quad \text{where } \boldsymbol{U} = \frac{\boldsymbol{r}}{2} \tag{11}$$

For a point magnetic dipole $\boldsymbol{\mu}$ associated with a nuclear magnetic spin, in atomic units the vector potential is given by

$$\boldsymbol{A} = \boldsymbol{\mu}\times\boldsymbol{U} \quad \text{where } \boldsymbol{U} = c^{-2}\frac{\boldsymbol{r}_N}{r_N^3} \tag{12}$$

where $\boldsymbol{r}_N$ is the electron nucleus distance, such that $\nabla\times\boldsymbol{A}$ yields the hyperfine field created by a nuclear spin. In this work, the Coulomb gauge is used for the vector potential. The hyperfine operators based on Eq. 12 have been derived previously in Refs. [44, 45] for the purpose of calculating indirect nuclear spin-spin coupling (J-coupling) tensors, and also by van Lenthe, Wolff, et al. in the context of NMR chemical shifts [46] and hyperfine tensor calculations based on a first-derivative paradigm [47]. The hyperfine and the static external magnetic field perturbation operators

have the same formal structure as long as one does not explicitly carry out derivatives of $\boldsymbol{U}$. In other words, differentiating $\hat{h}(\boldsymbol{B},\boldsymbol{S})$ with respect to B_u yields operators of the same formal structure as when differentiating $\hat{h}(\boldsymbol{\mu}_N,\mathbf{S})$ with respect to $\mu_{N,u}$. One simply replaces

$$\boldsymbol{U} = c^{-2}\frac{\boldsymbol{r}_N}{r_N^3} \quad \longleftrightarrow \quad \boldsymbol{U} = \frac{\boldsymbol{r}}{2} \tag{13}$$

The ZORA perturbation operators relevant for g-shifts that arise from external static magnetic fields were originally derived in Refs. [28, 46], but they can also be obtained easily by making the substitution (13) in the hyperfine operators for which we may take expressions from Refs. [44, 45]. The perturbation operator related to the electronic spin-orbit coupling is obtained from the ZORA spin-orbit operator which is the last term on the rhs of Eq. 7. The perturbation operators needed for g-tensor calculations read as follows:

1. For the external magnetic field:

$$\hat{h}^{(u)} = -\frac{i}{4}[\mathcal{K}(\boldsymbol{r}\times\nabla_u) + (\boldsymbol{r}\times\nabla_u)\mathcal{K}] \tag{14a}$$

2. For the spin-orbit coupling:

$$\hat{h}^{(v)} = \frac{i}{2}(\hat{\boldsymbol{p}}\mathcal{K}\times\hat{\boldsymbol{p}})_v \tag{14b}$$

3. For the bilinear external field—electron spin operator one obtains:

$$\hat{h}^{(u,v)} = \frac{1}{4}\{\delta_{uv}\boldsymbol{\nabla}\cdot(\mathcal{K}\boldsymbol{r}) - \nabla_u(\mathcal{K}r_v)\} \tag{14c}$$

In the last equation (unlike in Eq. 14a, b), the derivative acts only inside the operator, not to the function to its right. As in the works by SZ and LWA, the potential used in the operators is an approximation of the effective Kohn–Sham potential of the molecule. Therefore, contributions from the two-electron SO operator are included in the calculations in an approximate mean-field sense. Also as in the works by SZ and LWA, contributions from the spin—other-orbit (SOO) terms are not included. While SOO terms are expected to be of some relevance in g-tensor calculations on light atomic systems, their importance relative to one electron SO terms tends to rapidly diminish with increasing nuclear charge of the heavy atoms in a molecule [48–50]. For further details regarding the SOO term in g-tensor calculations and an implementation based on numerical integration which is compatible with our code see Patchkovskii et al. [51]. Based on fully origin invariant GIAO calculations, Patchkovskii et al. have shown that the SOO terms are usually quite small.

Often, g-tensors are calculated 'nonrelativistically' by starting with a nonrelativistic MO computations and using the Breit–Pauli terms for the perturbation operators. We may obtain the Pauli analogs of the perturbation operators from expanding $\mathcal{K}$ of Eq. 8 for small values of V,

$$\mathcal{K} \approx 1 + \frac{V}{2c^2} \tag{15}$$

and keeping the terms of order c^{-2}. Using this approximation, the operator (14b) changes to

$$\hat{h}^{(v)}(\text{Pauli}) = \frac{i}{4c^2}(\{\hat{\boldsymbol{p}}V\}\times\hat{\boldsymbol{p}})_v \tag{16}$$

where the curly brackets indicate that the derivative is taken only inside the operator. Compare with Eq. 28b of Schreckenbach and Ziegler (SZ) [23] which is the same operator (upon conversion of units, and considering the special case of a doublet system). SZ used explicitly the derivative of the XC potential in their implementation and approximated it with the Xα potential. We show in Sect. 2.5 that such derivatives, in particular those of $\mathcal{K}$ in the operators, can be easily avoided in calculations of the operator matrix elements.

The nonrelativistic limit, $\mathcal{K}\to 1$, of the bilinear operator (14c) is

$$\hat{h}^{(u,v)}(\text{nrel}) = \frac{1}{4}[\delta_{uv}\cdot 3 - \delta_{uv}] = \frac{1}{2}\delta_{uv}$$

Taking the expectation value in the sense of Sect. 2.2, and multiplying by $1/\beta_e$, yields with $\beta_e = 1/2$ a.u. an isotropic

$$g_{\text{nrel}} = \frac{1}{\beta_e}\langle\hat{h}^{(u,v)}\rangle = \delta_{uv}\frac{1}{\beta_e}\cdot\frac{1}{2}\cdot\left(\frac{n_\alpha - n_\beta}{2}\right)^{-1}(n_\alpha - n_\beta) = 2\delta_{uv}$$

Therefore, the nonrelativistic limit of this operator yields the free electron g-value of 2. If one adopts the Pauli approximation, in addition to the nonrelativistic limit $\hat{h}^{(u,v)}(\text{nrel})$ there arise the 'diamagnetic' or 'gauge correction' terms of the SZ paper from replacing $\mathcal{K}\to V/(2c^2)$,

$$\hat{h}^{(u,v)}(\text{Pauli}) = \frac{1}{8c^2}[\delta_{uv}\{\boldsymbol{\nabla}V\}\cdot\boldsymbol{r} - \{\nabla_u V\}r_v] \tag{17}$$

which match those reported by SZ, Eq. 29d, if the derivatives inside the operator act only on V but not on V and $\boldsymbol{r}$ which, as above, is indicated by the curly brackets. The additional terms involving the derivatives of $\boldsymbol{r}$ arising from the Pauli approximation of Eq. 14c, which have been eliminated from (17), yield an operator

$$\hat{h}^{(u,v)}(\text{Pauli-KE}) = \frac{1}{4c^2}[\delta_{uv}V] \tag{18}$$

This is not the same as the spin-Zeeman kinetic energy (KE) operator used by SZ and others, but its contribution to the g-tensor is the same. With a nonrelativistic reference electronic structure, assuming validity of the virial

theorem, $\langle V\rangle = -2\langle T\rangle = -\langle \hat{\boldsymbol{p}}^2\rangle$, the g-factor contribution from Eq. 18 is in atomic units

$$\frac{1}{\beta_e} S_z^{-1} \left\langle \frac{1}{4c^2}\delta_{uv} V \right\rangle = -\frac{1}{c^2}\delta_{uv}\langle \hat{\boldsymbol{p}}^2\rangle$$

for a doublet. Including prefactors, the transformed operator in the expectation value is the same as the Pauli kinetic energy correction term of SZ Eq. 29, who—as for other operators—already included the factors of $1/\beta_e$ and S_z^{-1} in the operator itself.

2.4 g-Tensor calculations with GIAOs

Equation 2 for the g-tensor assumes either a complete basis set or a basis set that is independent of the external magnetic field. However, magnetic properties are origin dependent if they are calculated with a finite standard AO basis set. In order to eliminate the origin dependence, one typically resorts to 'gauge-including atomic orbitals' (GIAOs) [36, 37]. In terms of a standard Gaussian-type or Slater-type atomic orbital (AO) basis set $\{\chi_s\}$, the GIAOs $\xi_s(\boldsymbol{B})$ are defined as

$$\xi_s(\boldsymbol{B}) = \chi_s \exp\left[-\frac{i}{2}(\boldsymbol{B}\times\boldsymbol{R}_s)\cdot\boldsymbol{r}\right] \tag{19}$$

where $\boldsymbol{R}_s$ is the center of the AO basis function χ_s (which is typically one of the nuclei in the molecule). One may extend this concept to time-dependent periodic magnetic field perturbations [52]. Using a GIAO basis set distributes the gauge origin of the magnetic vector potential over the molecule instead of keeping it fixed at the coordinate origin $\boldsymbol{r} = 0$.

Since the basis set is now dependent on $\boldsymbol{B}$, the magnetic field derivatives in Eq. 2 have to take this explicitly into account. One needs to develop the formalism in the AO basis, not in the MO basis as implied in Eq. 2. Let $\mathsf{C}^{(0)}$ be the coefficients for the unperturbed MOs in the AO basis, and $\mathsf{C}^{(u)}$ the coefficients of the magnetic field perturbed MOs. The parametrization adopted here is (using matrix notation)

$$\mathsf{C}^{(u)} = \mathsf{C}^{(0)}\mathsf{A}^{(u)} \tag{20}$$

where $\mathsf{A}^{(u)}$ is a matrix mixing occupied with occupied and unoccupied MOs in order to describe the perturbation by the magnetic field. We drop the perturbation index for unperturbed quantities (i.e. $\mathsf{C} = \mathsf{C}^{(0)}$, etc.) and consider the perturbation for one of the spins without explicitly writing the spin-index. For the occupied-occupied (oo) block,

$$\mathsf{A}_{\mathrm{oo}}^{(u)} = -\frac{1}{2}\mathcal{S}^{(u)} \tag{21}$$

where

$$\mathcal{S}^{(u)} = \mathsf{C}^{\dagger}\mathsf{S}^{(u)}\mathsf{C} \tag{22}$$

Here, S is the overlap matrix of the GIAO basis set. To first order,

$$S_{rs}^{(u)} = \frac{i}{2}\langle\chi_r|[\boldsymbol{r}\times(\boldsymbol{R}_s - \boldsymbol{R}_r)]_u|\chi_s\rangle \tag{23}$$

The occ-unocc part of the $\mathsf{A}^{(u)}$-matrix for each spin is obtained from

$$A_{ai}^{(u)} = \frac{\mathcal{F}_{ai}^{(u)} - \varepsilon_i \mathcal{S}_{ai}^{(u)}}{\varepsilon_i - \varepsilon_a} \quad a \in \text{unocc},\ i \in \text{occ} \tag{24}$$

Here, the ε's are the unperturbed scalar ZORA MO energies. The perturbed Fock-operator in the MO basis,

$$\mathcal{F}^{(u)} = \mathsf{C}^{\dagger}\mathsf{F}^{(u,0)}\mathsf{C} \tag{25}$$

is calculated from the GIAO matrix elements

$$F_{rs}^{(u)} = \langle\chi_r|\hat{h}^{(u)}|\chi_s\rangle + \sum_{t,w} P_{tw}^{(u,0)}[f_{HXC}]_{rstw} - \frac{i}{2}\langle\chi_r|(\boldsymbol{r}\times\boldsymbol{R}_r)_u\hat{F}|\chi_s\rangle + \frac{i}{2}\langle\chi_r|\hat{F}(\boldsymbol{r}\times\boldsymbol{R}_s)_u|\chi_s\rangle \tag{26}$$

Here, $\hat{F}$ is the Kohn–Sham Fock-operator of the unperturbed system and $[f_{HXC}]_{rstw} = [rs|r_{12}^{-1} + f^{XC}(1,2)|tw]$ is a matrix element of the Hartree and exchange-correlation (XC) linear response kernel in the unperturbed AO basis. For hybrid DFT, these terms also need to include exact-exchange contributions and related GIAO derivative terms, which have been implemented recently in the ZORA NMR code of the ADF package by Krykunov et al. [38].

The determination of the matrix $\mathsf{A}^{(u)}$ is common to all programs that calculate response properties related to perturbations by static external magnetic fields. In our code, we employ the scalar ZORA functionality of the NMR program of the ADF package, developed by Schreckenbach, Wolff, Ziegler, et al. [46, 53–55]. A new development in this code, made necessary for this work, has been the extension of the scalar ZORA branch for spin-unrestricted calculations. Thus, we can directly calculate the coefficient matrices $\mathsf{C}^{(u)\alpha}, \mathsf{C}^{(u)\beta}$ for α and β spin orbitals in a GIAO basis set, using the ZORA form of the orbital Zeeman operator, Eq. 14a, for the external field perturbation.

The calculation then proceeds as follows (based on an almost complete rewriting of the program, similar to what has been reported in Ref. [56] for the spin-orbit branch of the NMR code): As in the SZ paper, the g-tensor is split into a paramagnetic and diamagnetic ('gauge correction') component. Define the r, s elements of the scalar relativistic spin-density matrices in the AO basis,

$$P_{rs}^{(0)\alpha-\beta} = \sum_i n_i^{\alpha} C_{ri}^{(0)\alpha} C_{si}^{*(0)\alpha} - \sum_i n_i^{\beta} C_{ri}^{(0)\beta} C_{si}^{*(0)\beta} \tag{27a}$$

and

$$P_{rs}^{(u)\alpha-\beta} = \sum_i n_i^{\alpha} \left[C_{ri}^{(0)\alpha} C_{si}^{*(u)\alpha} + C_{ri}^{(u)\alpha} C_{si}^{*(0)\alpha} \right] - \sum_i n_i^{\beta} \left[C_{ri}^{(0)\beta} C_{si}^{*(u)\beta} + C_{ri}^{(u)\beta} C_{si}^{*(0)\beta} \right] \tag{27b}$$

where the n_i^{γ}, $\gamma = \alpha, \beta$, are the occupation numbers for the spin orbitals. For the magnetic field perturbation and real unperturbed orbitals, the perturbed spin-density matrix is imaginary.

The GIAO equivalent of Eq. 2, written in terms of g-shifts Δg, is then computed from

$$\Delta g_{uv}^{d} = \frac{4}{n_\alpha - n_\beta} \sum_{r,s} P_{rs}^{(0)\alpha-\beta} \left[\left\langle \chi_r | \hat{h}_s^{(u,v)} | \chi_s \right\rangle + \frac{i}{2} \left\langle \chi_r | [\boldsymbol{r}_s \times (\boldsymbol{R}_s - \boldsymbol{R}_r)]_u \hat{h}^{(v)} | \chi_s \right\rangle \right] \tag{28a}$$

for the diamagnetic terms, and

$$\Delta g_{uv}^{p} = \frac{4}{n_\alpha - n_\beta} \sum_{r,s} \left[P_{rs}^{(u)\alpha-\beta} \left\langle \chi_r | \hat{h}^{(v)} | \chi_s \right\rangle + P_{rs}^{(0)\alpha-\beta} \frac{i}{2} (\boldsymbol{R}_r \times \boldsymbol{R}_s)_u \left\langle \chi_r | \hat{h}^{(v)} | \chi_s \right\rangle \right] \tag{28b}$$

for the paramagnetic terms. Eq. 4 has been used for the effective spin. As in the work by SZ, going back to a suggestion by Fukui [57], the GIAO terms have been grouped in order to yield diamagnetic and paramagnetic tensors that are individually origin independent. In Eq. 28a, $\boldsymbol{r}_s = \boldsymbol{r} - \boldsymbol{R}_s$ is the distance with respect to basis function center no. s. Further, the operator $\hat{h}_s^{(u,v)}$ is a modified version of Eq. 14c where the position $\boldsymbol{r}$ is replaced by $\boldsymbol{r}_s$, i.e.

$$\hat{h}_s^{(u,v)} = \frac{1}{4} \{ \delta_{uv} \nabla \cdot (\mathcal{K} - 1) \boldsymbol{r}_s - \nabla_u (\mathcal{K} - 1) r_{s,v} \} \tag{29}$$

and $\mathcal{K}$ has been replaced by $(\mathcal{K} - 1)$ in order to subtract the free electron g-value from the result (see Sect. 2.3). For the implementation, it has been confirmed that using 1 instead of $\mathcal{K} - 1$ in the integrand of Eq. 28a, yields $2\delta_{uv}$ within the accuracy limits of the numerical integration. See Sect. 2.5 for further details.

2.5 Calculating matrix elements of the operators

The perturbation operators for g-tensors, like other magnetic perturbation operators in ZORA, involve derivatives of $\mathcal{K}$. Matrix elements of the operators are calculated in our implementation by numerical integration. In these numerical integrations, it is desirable to avoid the explicit calculation of the derivatives of $\mathcal{K}$. By using the turnover rule for the momentum operator and/or partial integration, the derivatives can be switched over to the basis functions χ_μ, χ_ν instead.

To calculate Δg_{uv} of Eqs. 28a and b, the matrix elements for the external magnetic field perturbation and all GIAO related terms needed to solve the CPKS equations and to obtain the perturbation matrices $\mathsf{A}^{(u)\gamma}$, $\gamma = \alpha, \beta$, of Sect. 2.4 are taken from the ZORA NMR code by Wolff et al. [46] and its recent hybrid DFT extension [38], after adapting it for spin-unrestricted calculations.

For the bilinear operator (14c), the derivatives are only acting in the operator. Thus, a simple partial integration shifts the derivative to the product of the basis functions instead, i.e.

$$h_{rs}^{(u,v)} = -\frac{1}{4} \int d^3 r \mathcal{K} \left[\delta_{uv} \boldsymbol{r} \cdot \nabla (\chi_r^* \chi_s) - r_v \nabla_u (\chi_r^* \chi_s) \right] \tag{30}$$

In our implementation, the numerical integration routine first calculates all u, v combinations of integrals over $\mathcal{K} r_v \nabla_u (\chi_r^* \chi_s)$ and then forms the isotropic and anisotropic combinations, which reduces the overhead in the loops in the integration code and renders the calculation particularly efficient. In the GIAO code the matrix elements of the operator (29) are needed instead, which can be computed from a straightforward modification of a code implementing the previous equation. We use $(\mathcal{K} - 1)$ in place of $\mathcal{K}$ in the integration in order to determine directly Δg shifts, as discussed above. The diamagnetic GIAO g-shift of Eq. 28a additionally requires matrix elements

$$G_{rs}^{uv} = \frac{i}{2} \langle \chi_r | [\boldsymbol{r}_s \times (\boldsymbol{R}_s - \boldsymbol{R}_r)]_u \frac{i}{2} [\hat{\boldsymbol{p}} (\mathcal{K} - 1) \times \hat{\boldsymbol{p}}]_v | \chi_s \rangle$$

By applying the turnover rule for the momentum operator, the integrand can be brought into a form suitable for numerical integration as

$$G_{rs}^{uv} = -\frac{1}{4} \int d^3 r (\mathcal{K} - 1) [\boldsymbol{r}_s \times (\boldsymbol{R}_s - \boldsymbol{R}_r)]_u [\nabla \chi_r \times \nabla \chi_s]_v - \frac{1}{4} \int d^3 r (\mathcal{K} - 1) \chi_r \{ \delta_{uv} (\boldsymbol{R}_s - \boldsymbol{R}_r) \cdot \nabla \chi_s - (\boldsymbol{R}_s - \boldsymbol{R}_r)_v \nabla_u \chi_s \} \tag{31}$$

For the matrix elements of the spin-orbit operator derivative $\hat{h}^{(v)}$, Eq. 16, there are various possibilities available. One of them is simply to apply the turnover rule for the momentum operator such that the matrix elements of the operator read

$$h_{rs}^{(v)} = \frac{i}{2} \int d^3 r \mathcal{K} \left[\{ \nabla \chi_r^* \} \times \{ \nabla \chi_s \} \right]_v \tag{32}$$

which is easy to implement in a code where $\mathcal{K}$ is available on a numerical integration grid. An alternative derivation uses the fact that

$$\mathcal{K} = 1 + (V/2c^2) + (V/2c^2)^2 + (V/2c^2)^3 + \cdots$$

In $\nabla\mathcal{K} \times \hat{\boldsymbol{p}} = \{\nabla\mathcal{K}\} \times \hat{\boldsymbol{p}}$, the constant term in the expansion of $\mathcal{K}$ does not contribute, and one can eliminate it easily by multiplying the series with $V/2c^2$, i.e.

$$\mathcal{K}\frac{V}{2c^2} = \mathcal{K} - 1 = \frac{V}{2c^2 - V}$$

Therefore, other ways of writing the spin-orbit operator matrix elements are

$$h_{rs}^{(v)} = \frac{i}{2}\int d^3r\mathcal{K}\frac{V}{2c^2}\left[\{\nabla\chi_r^*\} \times \{\nabla\chi_s\}\right]_v \tag{33a}$$

$$= \frac{i}{2}\int d^3r(\mathcal{K}-1)\left[\{\nabla\chi_r^*\} \times \{\nabla\chi_s\}\right]_v \tag{33b}$$

Numerical tests indicated that, compared to Eq. 32, the integrals witn $(\mathcal{K}-1)$ converge somewhat faster with the integration grid size. Therefore, the implementation uses Eq. 33b for the computation of the matrix elements of the SO operator spin derivatives.

3 Computational details

All computations were carried out with a developers version (pre-2010) of the Amsterdam Density Functional (ADF) package [35]. Geometry optimizations of the small molecules employed the BP86 functional [58–60] and a triple-zeta polarized STO all-electron basis set with two sets of polarization functions for all atoms (TZ2P from the ADF basis set library), and the scalar ZORA spin-unrestricted formalism. The BP86 functional was chosen for most of the optimizations as it is generally considered to model molecular geometries reasonably well [61]. The lanthanum DPA_3 complex was optimized at the scalar ZORA TZP/PBE level of theory, where TZP is a triple-zeta STO basis with one set of polarization functions for all atoms, and PBE is the Perdew–Burke–Ernzerhof (PBE [62]) generalized gradient approximation (GGA) functional. Calculations of the g-tensors were based on the optimized geometries and employed a relatively high setting of 7.0 for the numerical integration accuracy parameter in order to ensure well converged results. Test calculations on HgH showed that finite-nucleus corrections for the g-tensors were negligible and therefore all results reported in this work were obtained with the point nucleus approximation. Test calculations with the SZ code using the SOO implementation of Patchkovskii et al. [51] confirmed that SOO contributions to the g-tensors of our test set are small when compared, for instance, to the overall relative deviations between theory and experiment. We have thus decided to forgo an implementation of SOO terms in the second-order ZORA code for this initial benchmark study. The functionals used in the g-tensor calculations were the PBE non-hybrid functional and, for comparison, the PBE-based PBE0 hybrid functional [63, 64] which has a 25% fraction of exact exchange. The same TZ2P basis sets designed for ZORA computations as used in the geometry optimizations were used to determine the g-tensors in scalar and spin-orbit ZORA computations. The combination of unrestricted spin-orbit calculations with the first-order ZORA approach of LWA, which is not discussed in the paper describing the original implementation [28], was based on sets of three collinear computations with the spin quantization axis along x, y, and z, respectively [35]. For these calculations the ESR module of the ADF package was employed. Due to the way the g-tensor expressions were derived for the LWA approach, the ESR code attempts an educated guess for the sign of the principal g-tensor components. For further details regarding the first-order derivative code by LWA please see Ref. [28]. In some cases, based on comparisons with the second-order codes and literature data, the signs of the results obtained by us with the LWA code were changed and Δg values were obtained from the g-factors after the sign change was applied. The comparisons with the SZ approach employed the EPR module of the ADF package. This code allows for computations with the scalar relativistic Pauli Hamiltonian, which necessitated employing basis sets with frozen cores for heavy atoms. For this purpose, the large frozen core TZ2P basis set of the ADF basis set library has been utilized, except for NpF_6, UF_6^-, and UCl_6^-, where the smaller TZP analog was used. Second-order ZORA g-tensors were calculated with the new code described in Sect. 2. To generate the spin-restricted second-order ZORA results, spin-restricted calculations with fractional occupations of the frontier orbitals were carried out, followed by spin-unrestricted calculations using the 'restart' feature in ADF in which only the occupations were set but the orbitals were not allowed to relax. The orbitals and potential from this calculation were then used in the new code to obtain the g-tensor.

4 Results and discussion

4.1 Benchmark data for small molecules

A comparison of calculated and experimental isotropic Δg values is provided in Table 1. Isotropic Δg values obtained with the new linear response ZORA code described in Sect. 2 are listed under '2nd ZORA'. Data for the SZ second-order Pauli and the LWA first-order ZORA approaches were not taken from the literature but computed for this work using the same geometries, basis sets, and other technical settings as in the second-order ZORA computations (except for the use of frozen core basis sets in the SZ

Pauli computations, see Sect. 3). Note that for some g-tensors calculated using the ADF ESR program (LWA first-order approach, spin-orbit effects included variationally), the sign of some components have been changed. In general, results calculated with spin polarization are in reasonable agreement in both sign and order of magnitude with experiment and with computational data from the literature. Δg data calculated without spin polarization show a wide variability and in most cases deviate significantly from experiment. An exception is TiF_3 where the much larger magnitude of Δg from the spin-restricted calculations agrees better with experimental data. This has also been noted in Ref. [28] where it was pointed out that the experimental data were obtained from TiF_3 trapped in rare gas matrices. It is conceivable that medium effects rather than methodological shortcomings in the calculation are responsible for most of the differences between calculations and experiment. For the UCl_6^- molecule, in the spin-restricted second-order (scalar relativistic) calculations the gaps between occupied and unoccupied frontier orbitals are almost vanishing (<0.1 eV), and therefore the linear response calculation breaks down. We consider the result of this calculation numerically unreliable. For the spin-polarized calculations the orbital gaps of UCl_6^- remain finite, although both the SZ and our new ZORA second-order calculations overestimate the isotropic Δg shift of UCl_6^- with respect to experiment and other calculations. The first-order LWA approach appears to significantly underestimate Δg for this system. Overall, it is clear that spin polarization is an important influence and that its effects need to be considered when calculating electronic g-tensors.

The comparison of the ZORA spin-polarized first-order and second-order approach, columns 2 and 4 of Table 1, shows that the results agree quite well in most cases. Overall, despite its fundamental shortcomings in terms of variational stability, the Pauli second-order approach yields Δg values that are quite comparable to the second-order ZORA approach. Somewhat of a breakdown of the second-order linear response methods, visible both in ZORA and in the Pauli (SZ) data, is seen for the linear Hg radicals which is a consequence of the rotational symmetry along the molecular axis (see below for further discussion). On the other hand, the sign and order of magnitude of the huge Δg values in the actinide systems, a signature of very large spin-orbit coupling, is satisfactorily reproduced by the second-order approaches. Please note that the sign of the g-factors calculated for these systems with the first-order LWA approach had to be changed in order to match their accepted negative values [33, 34, 74]. In 1985, Case [74] reported relativistic DFT results (Xα functional) for isolated NpF_6 in an octahedral geometry and obtained good agreement with experiment data which was derived from measurements on crystalline samples. As far as we can deduce from the computational details provided in [74], a certain degree of parametrization went into the computations. Bolvin et al. [34] obtained excellent agreement with experimental data based on calculations with wave-function-based methods. In our DFT computations, the trend of increasingly negative Δg along the series NpF_6, UF_6^-, UCl_6^- is reproduced but overestimated. The overestimation of the Δg shift magnitudes in particular for UF_6^- and UCl_6^- is tentatively attributed to the known tendency of too strong covalent metal—ligand bonding obtained in DFT calculations, in particular with standard GGA functionals. It is quite interesting that the approaches where SO coupling is treated perturbationally are able to yield such large Δg shifts as obtained for the actinide halides. Case [74] already pointed out that the unpaired orbital in NpF_6 has a_{2u} symmetry in spin-free calculations and e_{3u} double group symmetry in spin-orbit calculations, where the latter but not the former can overlap with ligand s and p orbitals, and that such a qualitative change in bonding and its effects on EPR parameters might be difficult to treat only as a perturbation. The present DFT calculations yield orbital diagrams that agree well with those of Case's paper. The spin-polarized g-tensor calculations with the first-order LWA approach somewhat underestimate Δg for the actinide halide series and are seen not to reproduce the trend among the three systems. The spin-restricted LWA results agree well with experiment. A comparison of first- and second-order approaches for calculating the ligand hyperfine coupling constants should yield valuable additional information regarding the performance and limitations of perturbational spin-orbit treatments. Respective method development for ZORA using a second-order derivative approach is presently under way in our group.

The performance of the hybrid functional (PBE0 vs. PBE) is seen to be mixed. Minor changes toward or away from experiment are noted for some of the lighter atomic systems. A relatively large effect, percentage-wise, is obtained for TiF_3 where the PBE0 hybrid DFT result is closer to experiment (see also the discussions elsewhere in this section). For the mercury containing radicals, switching from PBE to PBE0 reduces the magnitude of Δg which, in particular for HgF, leads to a strong underestimation of the isotropic Δg-shift relative to experiment. For the actinide halide series, the hybrid functional increases the magnitude of Δg for NpF_6, away from experiment, but it helps to reduce the differences between the g-factors of the different complexes which is desirable.

Tables 2, 3, 4, 5 and 6 show more detailed data of the calculations for selected molecules. The values shown in these tables are the isotropic Δg, the tensor span

Table 1 Isotropic Δg shifts for small molecules, in ppt

	Spin-polarized				Spin-restricted		Exp.	Selected other calcs.
	1st (LWA) PBE	2nd Pauli (SZ) PBE	2nd ZORA		1st (LWA) PBE	2nd ZORA		
			PBE	PBE0		PBE		
CH_2	0.1383	0.1592	0.2057	0.1917		0.3030		
CH_3	0.4733	0.4915	0.5380	0.5080	0.6900	0.7227	0.10[a]	
HCO	−2.442	−2.397	−2.333	−2.298	−3.115	−3.018	−2.1[b]	−1.932[j]
HSiO	−1.820	−1.329	−1.696	−1.539	−1.622	−1.513	−1.3[c]	−1.748[j]
HSiS	−1.895	−1.204	−1.646	−1.463	−0.8607	−0.4020		−2.972[j]
SiOH	−24.13	−20.11	−24.13	−25.83	−135.1[†]	−119.6[†]		−31.96[j]
SiSH	−14.09	−11.52	−14.03	−15.12	−28.61	−27.14		−13.52[j]
HgH	−131.0	−100.3	−93.84	−91.66	−165.7	−116.1	−125[d]	−145.3[k]
HgF	−31.55	−18.06	−17.48	−13.02	−45.47	−26.97	−30.7[e]	−37.85[k]
TiF_3	−28.54	−29.87	−28.16	−39.94	−48.78	−47.02	−77.92[f]	−53.59[l]
NpF_6	−2,564*	−2,285	−2,761	−3,015	−2,565*	−4,030	−2,606[g]	−2,700[m,n,‡]
UF_6^-	−2,507*	−2,753	−3,330	−3,300	−2,803*	−5,400	−2,760[h]	−2,780[o,‡]
UCl_6^-	−2,205*	−4,551	−5,310	−4,990	−3,122*	−16,040[†]	−3,100[i]	−3,060[o,‡]

See Sect. 3 for computational procedures

LWA van Lenthe, Wormer, and van der Avoird, *SZ* Schreckenbach and Ziegler, *PBE* Perdew–Burke–Ernzerhof, *ZORA* zero order regular approximation

* Sign of g changed from ESR output

† Small HOMO-LUMO gap. See discussion

‡ Accurate to three significant figures

[a] Ref. [68]

[b] Ref. [70]

[c] Ref. [71]

[d] Ref. [72]

[e] Ref. [73]

[f] Ref. [75]

[g] Ref. [65]

[h] Ref. [66]

[i] Ref. [67]

[j] MRCI/TZVPP, 2nd order. Reference [69]

[k] DKS2-RI. Reference [31]

[l] 1st Order, spin-restricted ZORA, GGA/GIAO. Reference [28]

[m] Alternative value: $\Delta g = -2620$ SO-CASPT2/CAS3(7r). Reference [34]

[n] Dirac scattered-wave, 1st order. Reference [74]

[o] SO-CASPT2/CAS1(7r). Reference [34]

$\Omega = g_{33} - g_{11}$, and the skew $\kappa = 3(g_{\mathrm{iso}} - g_{22})/\Omega$ based on an ordering of the principal components $g_{33} \geq g_{22} \geq g_{11}$. Such data are commonly used to characterize chemical shift tensors [76] and are deemed to be useful in this work for the purpose of characterizing g-tensors. We do not provide such tables for the actinide systems. Owing to their octahedral geometry, the g-tensors for these systems are isotropic and therefore fully characterized by the data in Table 1.

The results for HCO are collected in Table 2. The comparison with experiment (Table 1) highlights the importance of spin polarization, which significantly improves the isotropic Δg and is seen to affect also the tensor span quite strongly. The data for HCO and HSiO (Table 3) indicate a relatively minor influence due from the functional (PBE vs. PBE0). In both cases, the agreement between the first-order and second-order ZORA approaches is quite close. The case of SiOH (Table 4) also emphasizes the importance of spin polarization. In this molecule, scalar relativistic effects appear to be strong enough to cause a significant difference between the ZORA and Pauli results, with ZORA being closer to reference data from the literature. The TiF_3 system (Table 5) has already

Table 2 Results for the HCO radical

HCO	Δg_{iso} (ppt)	Ω (ppt)	κ
Spin polarized			
1st (LWA) PBE	−2.442	12.42	−0.51
2nd Pauli (SZ) PBE	−2.397	12.47	−0.51
2nd ZORA PBE	−2.333	12.47	−0.52
2nd ZORA PBE0	−2.298	12.47	−0.50
Spin restricted			
1st (LWA) PBE	−3.115	15.53	−0.56
2nd ZORA PBE	−3.018	15.52	−0.57
Other calc[a]	−1.932	10.06	−0.55

[a] MRCI/TZVPP, 2nd Order. Reference [69]

Table 3 Results for the HSiO radical

HSiO	Δg_{iso} (ppt)	Ω (ppt)	κ
Spin polarized			
1st (LWA) PBE	−1.820	15.03	−0.33
2nd Pauli (SZ) PBE	−1.329	13.66	−0.27
2nd ZORA PBE	−1.696	15.08	−0.34
2nd ZORA PBE0	−1.539	14.95	−0.34
Spin restricted			
1st (LWA) PBE	−1.622	17.70	−0.28
2nd ZORA PBE	−1.513	17.72	−0.28
Other calc[a]	−1.748	12.25	−0.40

[a] MRCI/TZVPP, 2nd order. Reference [69]

Table 4 Results for the SiOH radical

SiOH	Δg_{iso} (ppt)	Ω (ppt)	κ
Spin polarized			
1st (LWA) PBE	−24.13	67.91	−0.93
2nd Pauli (SZ) PBE	−20.11	58.27	−0.95
2nd ZORA PBE	−24.13	69.82	−0.94
2nd ZORA PBE0	−25.83	75.43	−0.95
Spin restricted			
1st (LWA) PBE	−135.1	312.1	−0.98
2nd ZORA PBE	−119.6	356.14	−0.98
Other calc[a]	−31.96	94.93	−0.97

[a] MRCI/TZVPP, 2nd order. Reference [69]

been discussed above in some detail. The effect from the hybrid functional is more pronounced for this system, percentage-wise, than for the other molecules of Table 1. It has been pointed out that 3d transition metals are somewhat notorious in the context of response property calculations [22], in part due to the compactness of the 3d shell, which makes it important to consider electron correlation at a high level but also appears to aggravate the self-interaction problem in DFT. The singly occupied MO in TiF_3 is a

Table 5 Results for TiF_3

TiF_3	Δg_{iso} (ppt)	Ω (ppt)	κ
Spin polarized			
1st (LWA) PBE	−28.54	40.19	1.00
2nd Pauli (SZ) PBE	−29.87	42.50	1.00
2nd ZORA PBE	−28.16	40.20	1.00
2nd ZORA PBE0	−39.94	57.56	1.00
Spin restricted			
1st (LWA) PBE	−48.78	71.78	1.00
2nd ZORA PBE	−47.02	70.99	1.00
Other calc[a]	−53.59	78.70	1.00

[a] Spin-restricted ZORA, GGC/GIAO. Reference [28]

Table 6 Results for HgH

HgH	Δg_{iso} (ppt)	Ω (ppt)	κ
Spin polarized			
1st (LWA) PBE	−131.0	172.1	0.99
2nd Pauli (SZ) PBE	−100.3	150.2	1.00
2nd ZORA PBE	−93.84	140.7	1.00
2nd ZORA PBE0	−91.66	137.4	1.00
Spin restricted			
1st (LWA) PBE	−165.7	212.9	1.00
2nd ZORA PBE	−116.1	174.0	1.00
Other calc[a]	−145.3	186.1	1.00

[a] DKS2-RI. Reference [31]

metal centered 3d/4s hybrid (PBE: 73% $3d_{z^2}$, 20% $4s$. PBE0: 76% $3d_{z^2}$, 14% $4s$), and therefore the rather large influence from exact exchange seen in the g-tensor can be attributed to known difficulties of density functionals describing response properties that have their origin in the valence shell of a 3d metal.

For HgH (Table 6), the spin-polarized results show some variability, with the first-order treatment best predicting the g-tensor. The rather strong underestimation of the isotropic Δg magnitude with the second-order approaches goes along with a significant underestimation of the tensor span. The computed data for HgF show similar trends. The main problem is that in linear molecules such as HgH and HgF a sizable negative $\Delta g_{\parallel}$ tensor components is not obtained by these calculations. This issue has been discussed in detail in Refs. [20, 29] and early literature on g-tensors cited therein. With a spin-free unperturbed wavefunction, the scalar relativistic MOs are eigenfunctions of the $\hat{L}_{\parallel}$ operator, which has the same symmetry as the external field operator (14a) along the $\parallel$ direction. As a consequence, the MO matrix elements of this operator between different orbitals vanish along with the resulting linear response contribution to the $g_{\parallel}$. In the first-order

derivative approach, the orbitals are no longer eigenfunctions of the orbital angular momentum operator and comparatively large matrix elements for the perturbation may result. The very large Δg shifts calculated for NpF_6 and the other two actinide systems show that the breakdown is related to a combination of large spin-orbit coupling and symmetry and not simply related just to large magnitudes of the components of g itself.

Structural parameters of Hg compounds as a function of the basis set flexibility and the level of correlation treatment have recently been investigated by Kim et al. [77]. The optimized internuclear distance determined for HgF in this study (2.084 Å) falls within the range of optimized values reported by Kim et al. Additional computations of the Δg shifts of HgF were performed for a range of bond lengths from 1.96 to 2.24 Å in order to determine if the results are particularly sensitive to the bond length in this system. The bond length variations yielded changes of Δg of only up to 2.3 ppt, which is small compared to the difference between the second-order ZORA results and experiment.

4.2 Pseudocontact NMR chemical shifts in $[Ce(DPA)_3]^{3-}$

In addition to the previous set of small molecule benchmark calculations, we have considered axially symmetric lanthanide complexes of the formula $[Ln(DPA)_3]^{3-}$ (see Fig. 1) in order to investigate the electronic origin of paramagnetic effects on the NMR chemical shifts in the ligand sphere. Compared to the diamagnetic La(III) and Lu(III) DPA_3 complexes, the series of open shell lanthanide analogs exhibit more or less pronounced changes in the NMR chemical shifts of protons and ^{13}C nuclei in the ligands that must be attributed to the magnetic field created by, and spin polarization in the ligands induced by, the paramagnetic metal center [78]. We refer to these

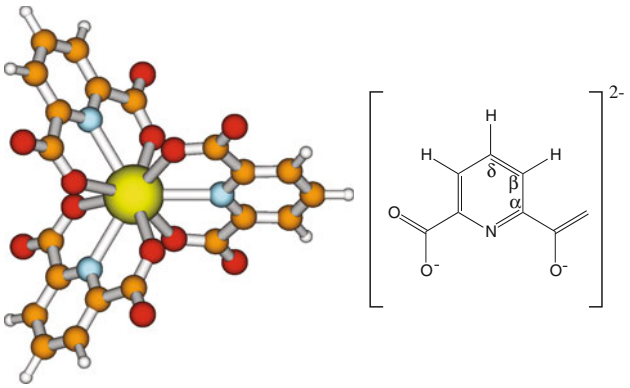

Fig. 1 Optimized structure of $[La(DPA)_3]^{3-}$ and labeling of some ligand atoms in the analogous $[Ce(DPA)_3]^{3-}$ complex

paramagnetic effects in the NMR spectrum by the acronym pNMR. In particular, it has been assumed that the ligand proton pNMR shifts are primarily of pseudocontact nature [78], which is a dipolar through-space interaction of the magnetic field created by the electron spin density at the paramagnetic metal center with a ligand atom's nuclear spin magnetic moment. It is appropriate to point to early theoretical work by Pyykkö et al. [79] related to pseudocontact shifts in lanthanide complexes. The pseudocontact shift of an axially symmetric system with spin S can be modeled based on optimized (or experimental) geometries and g-tensors, using the following equation as given by Bertini et al. [80] (SI units)

$$\delta^{PC} = \frac{\mu_0}{4\pi}\frac{\beta_e^2 S(S+1)}{3kT}\frac{3\cos^2\Omega - 1}{r^3}(g_\parallel + g_\perp)(g_\parallel - g_\perp)/3 \tag{34}$$

Here, r is the distance between the metal center and the nucleus of interest, and Ω is the angle between the principal symmetry axis and the vector drawn between the paramagnetic metal center and the nucleus of interest. Further, $g_\parallel$ and $g_\perp$ are the principal components of the g-tensor along and perpendicular to the threefold symmetry axis of the complex. The other symbols have their usual meaning. The results of the calculations are collected in Table 7. The geometry of the Ce complex was taken to be the same as that $[La(DPA)_3]^{3-}$. Since the NMR spectra were measured in aqueous solution, solvent effects were included in the calculations using the conductor-like screening model (COSMO) [82, 83]. The g-tensor was calculated using the second-order ZORA method presented in Sect. 2. Data in the footnotes of Table 7 show that the Pauli second-order approach yields significantly larger magnitudes of the Δg shifts which might indicate the onset of variational collapse. In Table 7, the pNMR effects estimated from the experimental data are listed as a combination of contact (C) and pseudocontact (PC) shifts. As already pointed out, the assumption for a complex such as $[Ce(DPA)_3]^{3-}$ is that the paramagnetic center is isolated because the 4*f* shell hardly participates in the bonding, and as a consequence the pNMR shifts in the ligand are predominantly of PC nature. The data in Table 7 show that the pNMR shifts for the protons H_β and H_δ are very well described by using a model for just the pseudocontact shifts, as previously predicted [78]. In order to cause such large PC shifts, the g-tensor has to be strongly anisotropic. For comparison, calculations that we performed with the SZ using a scalar relativistic calculation with the Pauli operator as a starting point yielded pNMR shifts of about twice the magnitude but otherwise of the right sign and of the right order of magnitude. Attempts to reproduce the PC shifts based on calculations with the LWA code were unsuccessful as the

Table 7 Results of the calculation of the pseudocontact shifts in $[Ce(DPA)_3]^{3-}$

Shift for	$[Ce(DPA)_3]^{3-}$	$[La(DPA)_3]^{3-}$	Exp. $\delta^{FC} + \delta^{PC}$	Calculated δ^{PC} (ppm)[a]
H_β	10.41	8.16	2.25	2.504
H_δ	10.53	8.24	2.29	2.273
C_α	159.95	150.48	9.47	11.43
C_β	137.78	126.83	10.95	4.792
C_δ	145.93	141.36	4.57	3.922
COO-	173.9	173.08	0.82	1.204

The NMR shielding of the related closed-shell $[La(DPA)_3]^{3-}$ system is taken to be equal to the diamagnetic 'orbital' shielding. Values calculated with $T = 298$ K in Eq. 34. Experimental data from Ref. [81]

[a] From this work: $g_\parallel = -0.2948\, g_\perp = -1.940$. From 2nd Pauli (SZ): $g_\parallel = -0.4641$, $g_\perp = -2.601$

predicted g-tensor was nearly isotropic. The cause of this apparent failure is presently unclear.

The carbon pNMR shifts calculated with ZORA agree less well with experiment than the proton shifts. For C_α and C_δ, the experimental trend is reproduced, but the shift for C_β deviates significantly from experiment. The discrepancy is likely due to additional small—but significant—contact shifts and possibly from pNMR contributions from low lying excited electronic states in the 4*f* manifold. The calculated PC shift is also sensitive to geometry parameters, both via r and Ω in Eq. 34, as well as via a geometry dependence in the g-tensor calculations. It should be noted that in Eq. 34 the value of δ^{PC} is zero for the 'magic' angle $\Omega = 54.74°$ and for $\Omega = 125.26°$. The calculated PC shift for atoms lying near these angles would be quite sensitive to the geometry. The value of Ω for the COO^- carbon in the optimized geometry is very close to 54.7 degrees and therefore the PC shift is small despite the proximity of this ligand atom to the paramagnetic center. We plan to investigate the various issues, such as geometry dependence and contact shift contributions, related to pNMR shifts in $[Ce(DPA)_3]^{3-}$ and similar systems in more detail in a subsequent study.

5 Summary and outlook

A method to calculate molecular g-tensors from second derivatives of the energy based on scalar ZORA DFT calculations has been developed. The implementation uses STO basis sets and is capable of non-hybrid and hybrid DFT computations. Isotropic Δg shifts were determined for light atomic radicals, for radicals containing Si and the TiF_3 system where scalar relativistic effects start to become important, for HgH and HgF where scalar relativistic effects are required in order to obtain a reasonable description of the chemical bonds [1], and for three actinide hexahalides for which the isotropic Δg shifts range in the (negative) thousands of ppt and are large enough to cause an overall negative sign of the g tensor. Except for TiF_3, the comparison of the PBE non-hybrid and the PBE0 hybrid functionals yielded somewhat mixed results, although it is likely that for large diverse test sets of molecules the hybrid will perform better on average. The direct comparison of g-tensor approaches based on first and second derivative methods based on the ZORA Hamiltonian confirmed the well-known breakdown of the second-order derivative method for linear heavy atom radicals. However, the fact that both the Pauli and the ZORA second-order methods were able to predict the several thousand ppt magnitude of Δg in systems such as NpF_6 indicates that a second derivative approach may nonetheless be a suitable computational tool for their study. An application of g-tensor calculations to the pNMR pseudocontact shifts in the ligand sphere of $[Ce(DPA)_3]^{3-}$ via Eq. 34 yielded reasonable agreement with experimental data. Future work will have to also consider contributions from contact shifts which, in simple cases, can be modeled separately with the help of calculations of the hyperfine tensor [3, 5, 84].

Acknowledgments This work has received financial support from the US Department of Energy, grant no. DE-SC0001136 (BES Heavy Element Chemistry Program). We thank the Center for Computational Research (CCR) at the University at Buffalo for their continued support of our research projects. JA thanks Dr. Serguei Patchkovskii for stimulating discussions.

References

1. Pyykkö P (1988) Chem Rev 88:563
2. Rieger PH (2007) Electron spin resonance. Analysis and interpretation. The Royal Society of Chemistry, Cambridge
3. Abragam A, Bleaney B (1970) Electron paramagnetic resonance of transition ions. Clarendon Press, Oxford
4. Harriman JE (1978) Theoretical foundations of electron spin resonance. Academic Press, New York
5. Moon S, Patchkovskii S (2004) In: Kaupp M, Bühl M, Malkin VG (eds) Calculation of NMR and EPR parameters. Theory and applications. Wiley-VCH, Weinheim, pp 325–338

6. Kaupp M, Köhler FH (2009) Coord Chem Rev 253:2376
7. Bertini I, Turano P, Vila AJ (1993) Chem Rev 93:2833
8. Rastrelli F, Bagno A (2009) Chem Eur J 15:7990
9. Jayatilaka D (1998) J Chem Phys 108:7587
10. Bolvin H (2006) Chem Phys Chem 7:1575
11. Autschbach J, Ziegler T (2003) Coord Chem Rev 238/239:83
12. Neese F (2001) J Chem Phys 115:11080
13. Lushington GH, Grein F (1996) Theor Chim Acta 93:259
14. Lushington GH, Grein F (1997) Int J Quantum Chem 106:3292
15. Lushington GH (2000) J Phys Chem A 104:2969
16. Moores WH, McWeeny R (1973) Proc R Soc Lond A 332:365
17. Ishii M, Morihashi K, Kikuchi O (1991) J Mol Struct (Theochem) 325:99
18. Vahtras O, Minaev B, Ågren H (1997) Chem Phys Lett 281:186
19. Kaupp M (2002) In: Lund A, Shiotani M (eds) EPR spectroscopy of free radicals in solids. Trends in methods and applications. Kluwer, Dordrecht
20. Patchkovskii S, Schreckenbach G (2004) In: Kaupp M, Bühl M, Malkin VG (eds) Calculation of NMR and EPR parameters. Theory and applications. Wiley-VCH, Weinheim, pp 505–532
21. Neese F (2009) Coord Chem Rev 253:526
22. Autschbach J (2010) In: Ishikawa J, Barysz M (eds) Relativistic methods for chemists. Challenges and advances in computational chemistry and physics, vol 10, chap 12. Springer, London, pp 521–598
23. Schreckenbach G, Ziegler T (1997) J Phys Chem A 101:3388
24. Patchkovskii S, Ziegler T (1999) J Chem Phys 111:5730
25. Malkina OL, Vaara J, Scimmelpfennig B, Munzarová M, Malkin VG, Kaupp M (2000) J Am Chem Soc 122:9206
26. Kaupp M, Reviakine R, Malkina OL, Arbuznikov A, Schimmelpfennig B, Malkin VG (2002) J Comput Chem 23:794
27. Hrobárik P, Malkina OL, Malkin VG, Kaupp M (2009) Chem Phys 356:229
28. van Lenthe E, Wormer PES, van der Avoird A (1997) J Chem Phys 107:2488
29. Belanzoni P, van Lenthe E, Baerends EJ (2001) J Chem Phys 114:4421
30. Malkin I, Malkina OL, Malkin VG, Kaupp M (2005) J Chem Phys 123:244103
31. Komorovský S, Repiský M, Malkina OL, Malkin VG, Malkin I, Kaupp M (2006) J Chem Phys 124:084108
32. Repiský M, Komorovský S, Malkin E, Malkina OL, Malkin VG (2010) Chem Phys Lett 488:94
33. Chibotaru LF, Ceulemans A, Bolvin H (2008) Phys Rev Lett 101:033003
34. Notter FP, Bolvin H (2009) J Chem Phys 130:184310
35. Baerends EJ, Ziegler T, Autschbach J, Bashford D, Bérces A, Bickelhaupt FM, Bo C, Boerrigter PM, Cavallo L, Chong DP, Deng L, Dickson RM, Ellis DE, van Faassen M, Fan L, Fischer TH, Fonseca Guerra C, Ghysels A, Giammona A, van Gisbergen SJA, Götz AW, Groeneveld JA, Gritsenko OV, Grüning M, Gusarov S, Harris FE, van den Hoek P, Jacob CR, Jacobsen H, Jensen L, Kaminski JW, van Kessel G, Kootstra F, Kovalenko A, Krykunov MV, van Lenthe E, McCormack DA, Michalak A, Mitoraj M, Neugebauer J, Nicu VP, Noodleman L, Osinga VP, Patchkovskii S, Philipsen PHT, Post D, Pye CC, Ravenek W, Rodríguez JI, Ros P, Schipper PRT, Schreckenbach G, Seldenthuis JS, Seth M, Snijders JG, Solà M, Swart M, Swerhone D, te Velde G, Vernooijs P, Versluis L, Visscher L, Visser O, Wang F, Wesolowski TA, van Wezenbeek EM, Wiesenekker G, Wolff SK, Woo TK, Yakovlev AL. Amsterdam density functional, SCM, theoretical chemistry. Vrije Universiteit, Amsterdam. http://www.scm.com
36. London F (1937) J Phys Radium 8:397
37. Ditchfield R (1974) Mol Phys 27:789
38. Krykunov M, Ziegler T, van Lenthe E (2009) J Phys Chem A 113:11495
39. van Lenthe E, Baerends EJ, Snijders JG (1993) J Chem Phys 99:4597
40. Philipsen PHT, van Lenthe E, Snijders JG, Baerends EJ (1997) Phys Rev B 56:13556
41. Nichols P, Govind N, Bylaska EJ, de Jong WA (2009) J Chem Theor Comput 5:491
42. Aquino F, Govind N, Autschbach J (2010) J Chem Theor Comput 6:2669
43. van Wüllen C (1998) J Chem Phys 109:392
44. Autschbach J, Ziegler T (2000) J Chem Phys 113:936
45. Autschbach J, Ziegler T (2000) J Chem Phys 113:9410
46. Wolff SK, Ziegler T, van Lenthe E, Baerends EJ (1999) J Chem Phys 110:7689
47. van Lenthe E, van der Avoird A, Wormer PES (1998) J Chem Phys 108:4783
48. Okada S, Shinada M, Matsuoka O (1990) J Chem Phys 93:5013
49. Ishikawa Y, Nakajima T, Hada M, Nakatsuji H (1998) Chem Phys Lett 283:119
50. Vaara J, Ruud K, Vahtras O, Ågren H, Jokisaari J (1998) J Chem Phys 109:1212
51. Patchkovskii S, Strong RT, Pickard CJ, Un S (2005) J Chem Phys 122:214101
52. Krykunov M, Autschbach J (2005) J Chem Phys 123:114103
53. Schreckenbach G, Ziegler T (1997) Int J Quantum Chem 61:899
54. Schreckenbach G, Ziegler T (1998) Theor Chem Acc 99:71
55. Wolff SK, Ziegler T (1998) J Chem Phys 109:895
56. Autschbach J (2008) J Chem Phys 128:164112
57. Fukui H (1987) Magn Res Rev 11:205
58. Becke AD (1988) Phys Rev A 38:3098
59. Perdew JP (1986) Phys Rev B 33:8822
60. Perdew JP (1986) Phys Rev B 34:7406
61. Ahlrichs R, Furche F, Grimme S (2000) Chem Phys Lett 325:317
62. Perdew JP, Burke K, Ernzerhof M (1996) Phys Rev Lett 77:3865
63. Ernzerhof M, Scuseria GE (1999) J Chem Phys 110:5029
64. Adamo C, Barone V (1999) J Chem Phys 110:6158
65. Hutchison CA Jr, Weinstock B (1960) J Chem Phys 32:56
66. Masson JP, Desmoulin JP, Charpin P, Bougon R (1976) Inorg Chem 15:2529
67. Selbin J, Ortego JD, Gritzner G (1968) Inorg Chem 7:976
68. Jen CK, Foner SN, Cochran EL, Bowers VA (1958) Phys Rev 112:1169
69. Grein F (2004) Chem Phys 296:71
70. Holmberg RW (1969) J Chem Phys 51:3255
71. Zee RJV, Ferrante RF, Weltner W Jr (1985) J Chem Phys 83:6181
72. Knight LB Jr, Weltner W Jr (1971) J Chem Phys 55:2061
73. Knight LB Jr, Fisher TA, Wise MB (1981) J Chems Phys 74:6009
74. Case DA (1985) J Chem Phys 83:5792
75. De Vore TC, Weltner W (1977) J Am Chem Soc 99:4700
76. Harris RK, Becker ED, Cabral De Menezes SM, Granger P, Hoffman RE, Zilm KW (2008) Pure Appl Chem 80:59
77. Kim J, Ihee H, Lee YS (2010) J Chem Phys 133:144309
78. Desreux JF, Reilley CN (1976) J Am Chem Soc 98:2105
79. Golding RM, Pyykkö P (1973) Mol Phys 26:1389
80. Bertini I, Luchinat C, Parigi G (2002) Prog Nucl Mag Res Sp 40:249
81. Ouali N, Bocquet B, Rigault S, Morgantini PY, Weber J, Piguet C (2002) Inorg Chem 41:1436
82. Klamt A, Schüürmann G (1993) J Chem Soc Perkin Trans 2:799
83. Pye CC, Ziegler T (1999) Theor Chem Acc 101:396
84. Hrobárik P, Reviakine R, Arbuznikov AV, Malkina OL, Malkin VG, Köhler FH, Kaupp M (2007) J Chem Phys 126:024107